PRECIPITATION OF RADIATION BELT ELECTRONS BY MAGNETOSPHERICALLY REFLECTED (MR) WHISTLERS

D.Jasna, U.S.Inan and T.F.Bell

We use test particle simulation model based on gyro-averaged equations of motion to study the influence of oblique Magnetospherically Reflected (MR) whistlers on the rear-loss-cone distribution function of radiation belt electrons. We find that MR whistlers originating in lightning can resonantly interact with radiation belt electrons over a broad range of L-shells and precipitate higher energy electrons from lower L-shells. Electrons in the energy range of 1–2.6 MeV are precipitated from L = 2, whereas from L = 4 the precipitated electron energy range is 150–220 keV. The precipitated differential electron flux, due to this interaction, is higher for higher L-shells, and the maximum value ranges from $\Phi_{E_{prec}}(1.11\ \text{MeV}) = 5.2 \times 10^{-4}$ el/cm^2·s·keV at L = 2 to $\Phi_{E_{prec}}(173\ \text{keV}) = 4.6 \times 10^{-1}$ el/cm^2·s·keV at L = 4. The lifetimes of radiation belt electrons in a given magnetic flux tube around the L-shell on which the interaction takes place are found to be of the order of several days, comparable to lifetimes corresponding to electron loss induced by hiss, which was heretofore assumed to be the dominant loss mechanism [1]. The minimum electron lifetimes vary from 2.47 days for E = 1.11 MeV electrons at L = 2 to 4.64 days for E = 173 keV electrons at L = 4.

INTRODUCTION

Past investigations of resonant whistler-mode wave–particle interactions have recognized their importance in the loss of radiation belt electrons (e.g., [2]). Experimental observations have shown that ionospheric effects of precipitated electrons, such as sub-ionospheric VLF perturbations, X-ray emissions, or photoemissions can often be correlated with natural ducted VLF waves (whistlers, chorus emissions, noise bursts, etc.) [3–11]. In particular, the ionospheric signatures of the scattering of energetic electrons out of the radiation belts in cyclotron resonant interactions with lightning-generated ducted (i.e., parallel propagating) whistlers have been both theoretically studied in detail (e.g. [12]) and are now commonly observed [13, 14, and references therein]. As a measure of the effectiveness of this interaction, precipitated energetic electron fluxes have been theoretically estimated and compared with experimental data [15, 16, 17].

However, the bulk of the wave energy injected into the magnetosphere by lightning discharges propagates in the non-ducted mode. Although non-ducted waves may be less efficient than ducted waves in pitch angle scattering and precipitation of electrons in a single encounter cyclotron resonant

interaction (due to elliptical polarization of non-ducted waves versus circular polarization of ducted waves), their overall effect on radiation belt electron precipitation is yet to be ascertained.

MAGNETOSPHERICALLY REFLECTED (MR) WHISTLERS

Non-ducted (oblique) whistler mode waves originating in lightning discharges are often found to undergo multiple reflections between hemispheres. These reflections occur at points where the wave frequency matches f_{LHR} the local lower hybrid resonance frequency [18].

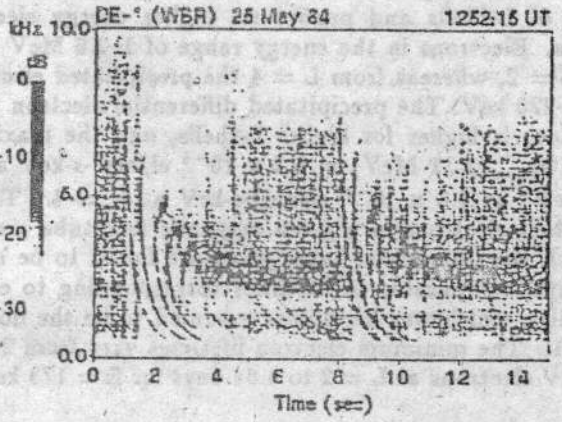

Fig.1. MR whistlers observed on the DE–1 satellite. The examples are given in the form of a typical frequency vs time spectrogram with the shading representing the intensity of the recorded signal. Two whistler events originating in two successive lightning flashes, ~ 8 s apart, ate shown, each initiating a sequence of MR components. After very pronounced dispersion of the first four hops of both whistlers, the hops begin to merge into each other to form a relatively narrow band signal lasting for about 2 s.

Figure 1 shows examples of MR whistlers observed on the DE–1 satellite. The format is one of a typical frequency vs time spectrogram with the density of the shading representing the intensity of the recorded signal. Two whistler events originating in two successive lightning flashes (in this case ~ 8 s apart) are shown, each initiating a sequence of MR components. The first few (four) hops of both whistlers show very pronounced dispersion after which the hops begin to merge into each other to form a long enduring relatively narrowband signal. The duration of the narrowband part of the signal for this example is about 2 s. Although the total duration of each MR event is ~ 10 s for the cases shown, MR whistlers are known to last for as long as 100 s [19].

Both ducted and MR (oblique) whistlers are generated by lightning discharges. It should be noted that non-ducted whistlers do not require the presence of any specific density structures (e.g., ducts) for their propagation. They generally occupy larger regions of the magnetosphere [20]. On this basis,

although the statistics of the occurrence rates of non–ducted whistlers are not well documented, it may safely be assumed that they occur at least as often as ducted whistlers. The ducted whistler rate depends on the time of the year and time of the day and varies from 0.3 whistlers per minute for an average summer day to 22 whistlers per minute for an average winter night [21]. For an extremely active day, the ducted whistler rate can be as high as 195 whistlers per minute, but year–round average is 6 whistlers per minute.

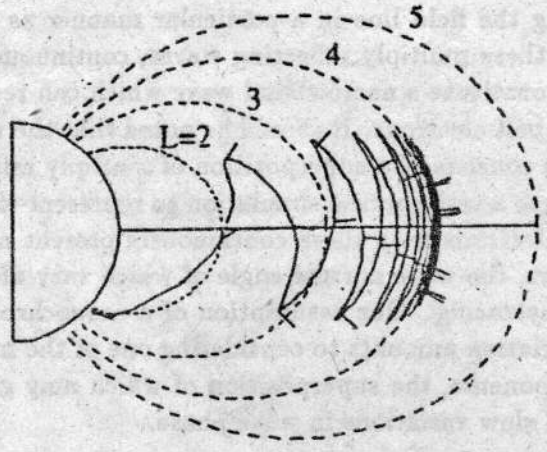

Fig.2. Sample raypath for an MR signal. The raypath for a $f = 0.33$ kHz wave injected at 400 km altitude, vertically upwards from the southern hemisphere at L = 2, propagating to higher L-shells by reflecting back and forth between hemispheres and eventually settling down at L ~ 4.

The magnetospheric reflection of oblique whistler mode waves can be effectively studied by raytracing. Here we utilize the Stanford VLF raytracing code (e.g., see [22]). The example in Figure 2 shows a $f = 0.33$ kHz wave injected vertically upwards from the southern hemisphere at L = 2. The ray travels vertically upwards reflecting back and forth between the hemispheres as expected and eventually settles down at L ≅ 4. More extensive raytracing studies [19] show that the L-shell at which the whistler wave settles down depends strongly on the wave frequency, but is relatively independent of the injection latitude or initial wave propagation direction. The frequency of the whistler wave vs L-shell of settlement as obtained from raytracing is plotted in Figure 3.

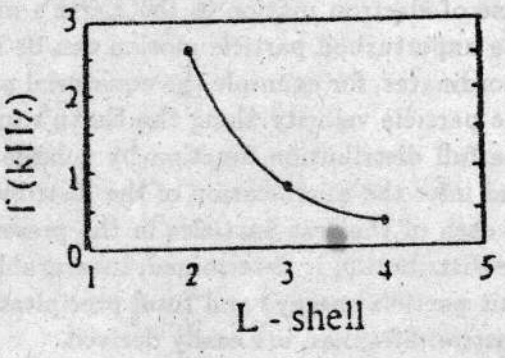

Fig.3. The frequency of the MR whistler wave vs L-shell of settlement. This result is derived on the basis of simulated raypaths as shown on Figure 2.

To summarize, MR whistlers are oblique whistler mode waves injected into the magnetosphere by lightning, they can endure in the magnetosphere for as long as 100 s each, and after several (5–6) reflections the raypaths settle down into a multiply reflecting pattern at an L-shell uniquely corresponding ($f \approx f_{LHR}$) to the signal frequency. Thus, at any given L-shell, we can expect accumulation of oblique whistler mode wave energy at the corresponding frequency. The wave normal angle of the multiply reflecting waves slowly varies with latitude along the field line in a particular manner as dictated by raytracing. As such, these multiply reflecting waves, continuously present along the given L-shell constitute a narrowband wave which can resonantly interact with the radiation belt electrons. It should be noted that the wave distribution along the field line consists of a superposition of multiply reflecting waves. In the following, we use a test particle simulation to represent the interactions of a distribution of electrons with these continuously present nearly monochromatic MR whistlers, the wave normal angle of which vary along the field line as described by raytracing. Our assumption of a monochromatic wave with specified phase variation amounts to considering one of the many multiply reflecting wave components, the superposition of which may generate standing wave patterns and slow variations in wave phase.

ELECTRON VELOCITY SPACE

In general, electron velocity space is three dimensional. For the special case of electron motion in the Earth's magnetosphere, important features of the unperturbed particle motion can be described by only two velocity space coordinates, for example the equatorial pitch angle α_{eq} and the component of the particle velocity along the Earth's magnetic field line v_{zeq}. We represent the full distribution function by a large number of individual test particles and infer the modification of the distribution from the simulated trajectories of each of the test particles in the presence of the wave. Once a new particle distribution is determined, measurable quantities such as differential (per unit particle energy) and total precipitated particle fluxes and radiation belt electron lifetimes, are easily derived.

Figure 4 shows a single test electron scattering in $v_{zeq} - \alpha_{eq}$ velocity space. Note that in the absence of the wave, the trajectory of a test electron moving in the Earth's magnetic field would be a single point in $v_{zeq} - \alpha_{eq}$ space. Due to the interaction with the wave, the electron trajectory in velocity space evolves along a curve with initial and final points corresponding to the initial and final velocity space coordinates. Since the wave forces acting on the particle are functions of the initial electron phase η (the third velocity coordinate that determines the direction of the electron velocity perpendicular to the Earth's magnetic field), electron trajectories and their final points in velocity space

depend on the initial η [23, 24].

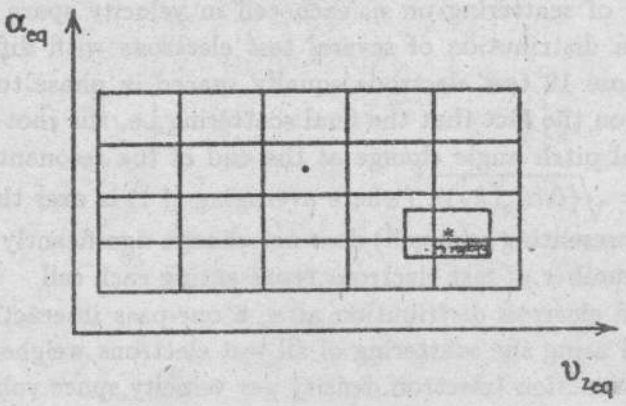

Fig.4. A single test electron scattering in velocity space. The schematic shows the initial and final points of the test electron trajectory in the velocity space. Electron population from the initial cell represented by the test electron is scattered into the four adjoining cells as represented by the cell corresponding to final point on the electron trajectory. The number of electrons scattered into any of the four adjoining phase cells is proportional to the area of the final cell that overlaps the corresponding cell.

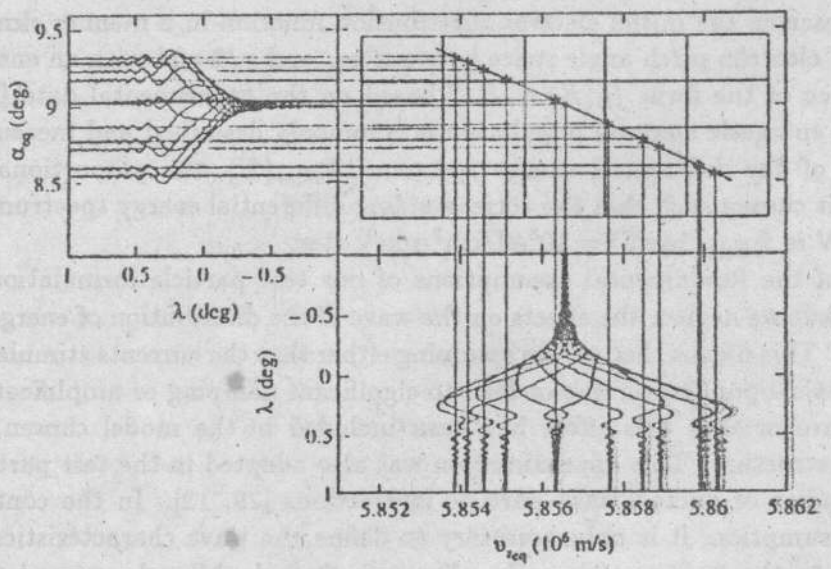

Fig.5. Test electron trajectories in the velocity space. Trajectories of the twelve test electrons with different initial phases, originating at the same initial point in velocity space are represented in velocity space as $\alpha_{eq}(v_{z_{eq}})$ and as the velocity space coordinates dependence on geomagnetic latitude namely $\alpha_{eq}(\lambda)$ and $v_{z_{eq}}(\lambda)$.

Figure 5 shows twelve different electron trajectories corresponding to 12

electrons with different initial phases, originating at the same initial point in velocity space (i.e., having the same initial α_{cmeq} and $v_{z_{eq}}$. In view of this dependence of scattering on η, each cell in velocity space needs to be represented by a distribution of several test electrons with different initial phases. We choose 12 test electrons equally spaced in phase to represent a given cell based on the fact that the final scattering i.e. the root–meansquare value of the final pitch angle change at the end of the resonant interaction, namely $\overline{\Delta\alpha_{eq_f}} = \sqrt{\langle \Delta\alpha_{eq}^2(\lambda_f)\rangle}$, (where averaging ($\langle\ \rangle$) is over the number of test electrons representing each cell) does not change significantly with further increase of the number of test electrons representing each cell.

The modified electron distribution after a one-pass interaction with the wave is obtained using the scattering of all test electrons weighed by the initial distribution function (electron density per velocity space volume) and its dependence on the velocity space coordinates [i.e., $f(v_{z_{eq}}, \alpha_{eq})$].

INITIAL CONDITIONS AND ASSUMPTIONS

In the inner magnetosphere ($L \leq 6$), we use the diffusive equilibrium background 'cold' plasma density model [25, 26] and centered dipole field as a model of the Earth's magnetic field.

We describe the initial electron distribution function in a manner similar to that of electron pitch angle space between α_{1c} and $\pi/2$ and with an energy dependence of the form $f_E(E) \propto E^{-3}$ based on the experimental data [28]. Since the energetic electron population is commonly described and measured in terms of the differential energy spectrum $\Phi_{E_{\text{diff}}}(E)$, the proportionality constant is chosen such that the corresponding differential energy spectrum at $E = 1$ keV is $\Phi_{E_{\text{diff}}}(1\,\text{keV}) = 10^8$ el/cm^2·s·keV·ster.

One of the fundamental assumptions of our test particle formulation is the fact that we neglect the effects on the wave of the distribution of energetic electrons. This means that we are assuming either that the currents stimulated in the particle population do not lead to significant damping or amplification of the wave or that this effect has been included in the model chosen for the wave structure. This approximation was also adopted in the test particle model studies of ducted wave–particle interactions [29, 12]. In the context of this assumption, it is only necessary to define the wave characteristics as an input to the test particle code. For non–ducted obliquely propagating waves, taking the wave as a predefined structure and neglecting the effects of the energetic particles on the wave is probably an even better approximation, since growth and emission triggering by non–ducted waves is observed much less often [30].

In our modeling, then, we assume the wave to be monochromatic (single frequency), and propagating at a given angle ψ with respect to the magnetic

field. With the wave frequency ω and wave normal angle ψ specified, all properties of the wave are defined in terms of the local cold plasma parameters. The properties (dispersion relation, polarization of the wave fields, group velocity) of the electromagnetic waves that are supported by the cold, infinite, homogeneous, collisionless plasma in the presence of the external homogeneous, static magnetic field are derived from Maxwell's equations [31]. The magnetosphere is not a homogeneous medium since both the plasma density and magnetic field (and therefore plasma and cyclotron frequencies of the kth species, ω_{pk} and ω_{Hk} respectively) vary in space. Fortunately, these spatial variations are generally small over the distance of the order of the wavelength, so that at any given point, the wave propagation can be represented using the slowly varying approximation (WKB) in which the wave is assumed to have the same characteristics as those of a wave traveling in a homogeneous medium having the same refractive index. The Poynting flux (power density) of the slowly varying wave was also assumed to be constant during its interaction with the radiation belt electrons, although the wave normal angle ψ was allowed to slowly vary with latitude as dictated by raytracing. The assumed constant Poynting flux value was used to calculate the wave field components at different points along the field line.

The precipitated differential electron energy spectrum caused by the electron–wave interaction $\Phi_{E_{prec}}(E)$ is used to infer the electron lifetimes in a given magnetic flux tube subject to certain assumptions as discussed below. We note in this context that the precipitated differential energy spectrum may change as a function of time both because of temporal drifts, or because of variations in the parameters of the wave interacting with the electrons. For the purpose of estimating electron lifetimes $\tau(E)$, we assume that the precipitated differential energy spectrum remains constant in time, i.e., $\Phi_{E_{prec}}(E,t) \sim \Phi_{E_{prec}}(E)$. We define N_f as the number of energetic electrons with a given energy per unit energy in a flux tube, per unit area of a tube cross section, at the equator so that the SI unit of the variable N_f is el/m^2-J. We assume that N_f decays exponentially in time as a result of the resonant scattering due to the electron–wave interaction $N_f(E,t) = N_f(E)\exp(-t/\tau(E))$ while $\partial N_f(E,t)/\partial t = -\Phi_{E_{prec}}(E,t) = -\Phi_{E_{prec}}(E)$ so that the lifetime of the electrons in a given tube is $\tau(E) = N_f(E)/\Phi_{E_{prec}}(E)$.

Note that the electron lifetimes defined above are derived for the electron population confined to a narrow flux tube around the field line where the interaction takes place. The extent to which this loss process contributes to the electron lifetimes on a global scale depends on the extent of magnetospheric regions illuminated by the waves, since similar scattering processes would be expected in all regions where the oblique waves are present. Experimental data indicates that magnetospheric regions illuminated by whistlers from a given thunderstorm center may extend to many tens of degrees in longitude around that of the storm center [20].

ELECTRON PRECIPITATION BY MR WHISTLERS

We now investigate the interaction between radiation belt electrons and MR whistlers in the equatorial region at three typical L-shells. The Poynting flux of the whistler waves was assumed to be $S = 113$ pW/m^2 corresponding to the intensity of a $f = 6.82$ kHz ducted wave ($\psi = 0^0$) with $B_w = 5$ pT in the equatorial plane at $L = 4$. The frequencies of the waves that settle down at the chosen L-shells and the dependence of their wave normal angle ψ on the geomagnetic latitude are determined using the Stanford raytracing simulation code. The $\psi(\lambda)$ used for simulation represents best-fits to the numerical results obtained from raytracing. The variation of wave normal angle along the field line $\psi(\lambda)$ is slow enough so that the wave can be considered monochromatic in the WKB sense.

We now study the resonant interaction between these monochromatic MR signals and radiation belt electrons represented by the distribution function as defined earlier, using the test particle simulation model.

Figure 6 shows the near loss cone electron distribution function resulting from a one-pass interaction with a 0.33 kHz oblique whistler wave at $L = 4$. Local maxima and minima in electron scattering occur due to the constructive and destructive interference between the two resonant encounters (on both sides of the equator) of the particles with the wave. Maximum penetration into the loss cone ($\sim 5 \times 10^{-4}$ deg) occurs for $v_{z_{eq}} = 198.4 \times 10^6$ m/s.

The distribution functions similar to that shown in Figure 6 and which result from a one-pass interactions with the wave are also computed for $L = 2$ and 3 and are subsequently used to calculate the precipitated differential electron spectra as shown in Figure 7 for all three L-shells. In general, MR whistler components which settle down on higher L-shells resonantly interact with and scatter lower energy electrons. For example, a 0.33 kHz whistler wave at $L = 4$ scatters electrons in the 150–220 keV range, whereas the 2.6 kHz MR whistler component that settles down at $L = 2$ scatters electrons in the 1–2 MeV energy range. Precipitated differential electron flux is in general higher for lower energy electrons that are scattered on higher L-shells. Maximum value of the precipitated differential electron flux at $L = 4$ is $\Phi_{E_{prec}}(173\,\text{keV}) = 4.6 \times 10^{-1}$ el/cm^2·s·keV. Corresponding total precipitated energy fluxes are $Q(L = 2) = 0.48 \times 10^{-9}$ J/m^2·s, $Q(L = 3) = 2.66 \times 10^{-9}$ J/m^2·s, $Q(L = 4) = 3.14 \times 10^{-9}$ J/m^2·s and are generally higher for higher L-shells.

The electron lifetimes corresponding to the precipitated fluxes of Figure 7 and calculated using the definitions and assumptions described earlier are given as a function of electron energy in Figure 8. The minimum lifetimes of the electrons with the corresponding energy that are scattered by MR whistlers are of the order of several days and do not differ significantly for interactions on different L-shells. The minimum electron lifetimes vary from 2.47 days for

E = 1.11 MeV electrons at L = 2 to 4.64 days for E = 173 keV electrons at L = 4.

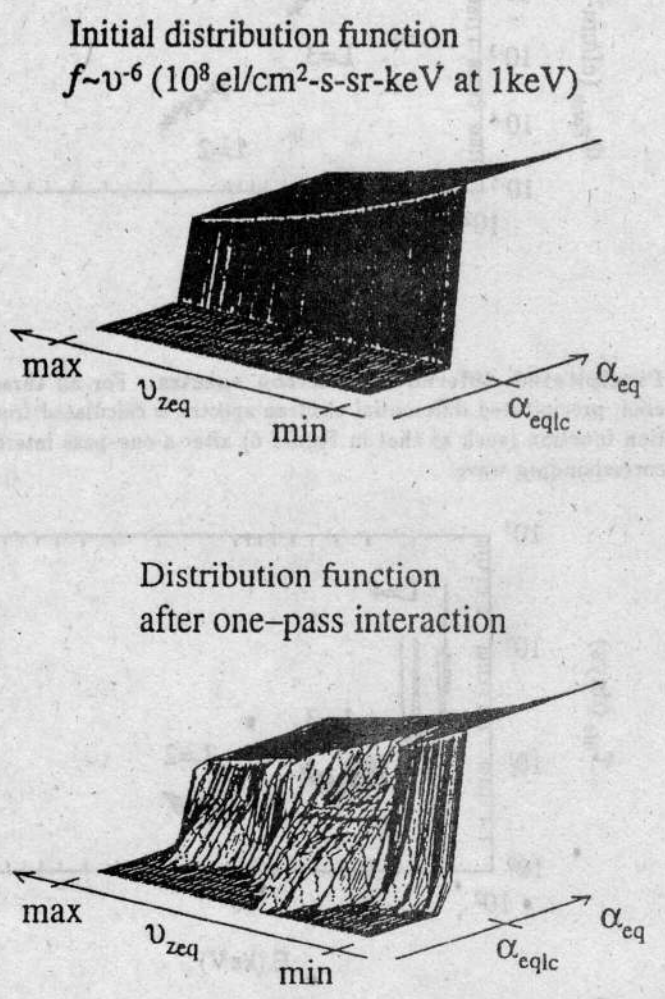

Fig.6. THe initial and final near–loss–cone electron distributions for a one–pass interaction with 0.33 kHz whistler wave at L = 4. Local maxima and minima in electron scattering occur due to the constructive and destructive interference between the two resonant encounters of the distribution with the wave.

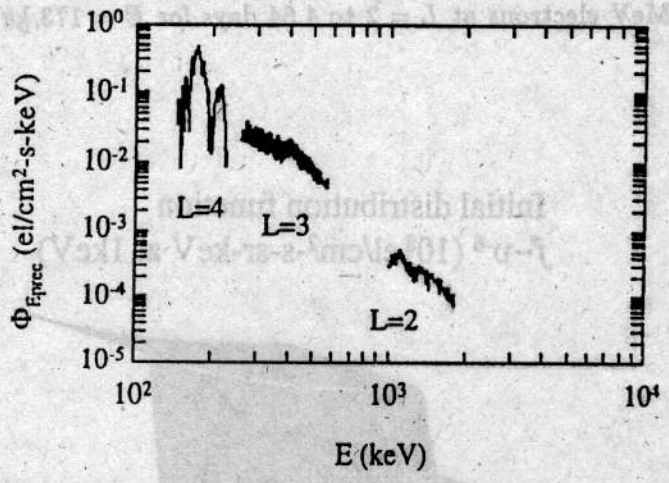

Fig.7. Precipitated differential electron spectra. For all three cases considered, precipitated differential electron spectra is calculated from the distribution function (such as that in Figure 6) after a one-pass interaction with the corresponding wave.

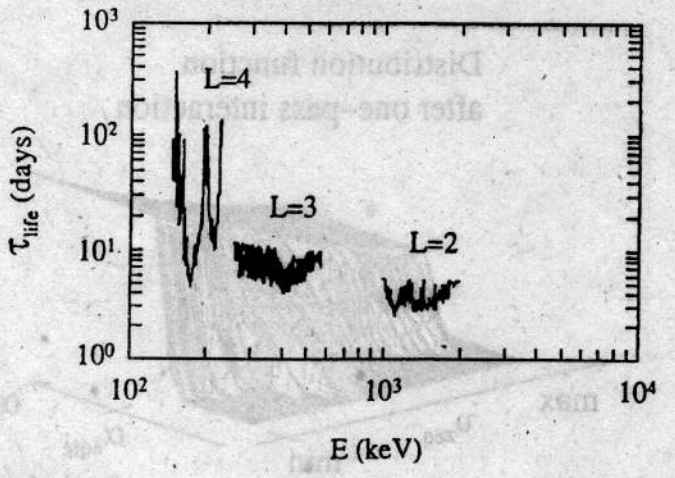

Fig.8. Electron lifetimes. Precipitated differential electron spectra are used to calculate electron lifetimes as discussed in the text.

In Figure 9 we compare our lifetime estimates with those due to cyclotron resonant scattering by whistler mode hiss following large magnetic storms [1]. Interaction between radiation belt electrons and hiss causes precipitation and loss from $L = 3$ and 4 of electrons in a broader energy range than that due to the resonant electron-MR whistler interaction. At $L = 3$ and 4 electron lifetimes due to hiss induced losses are smaller than the electron lifetimes due to resonant electron-MR whistler interaction. However, a $L = 2$ MR whistlers

can contribute more than hiss to the electron loss from the radiation belts. Note that the results given by [1] are calculated based on the assumption of the continuous presence of a wide band oblique whistler mode signal throughout the entire plasmasphere. In order to be able to compare the two, we also assumed the continuous presence of coherent, narrowband oblique whistler mode signal throughout the entire plasmasphere. However, our results can be scaled to more realistic values by simple multiplication once the ratios for spatial and temporal presence of the MR whistlers throughout the plasmasphere are available.

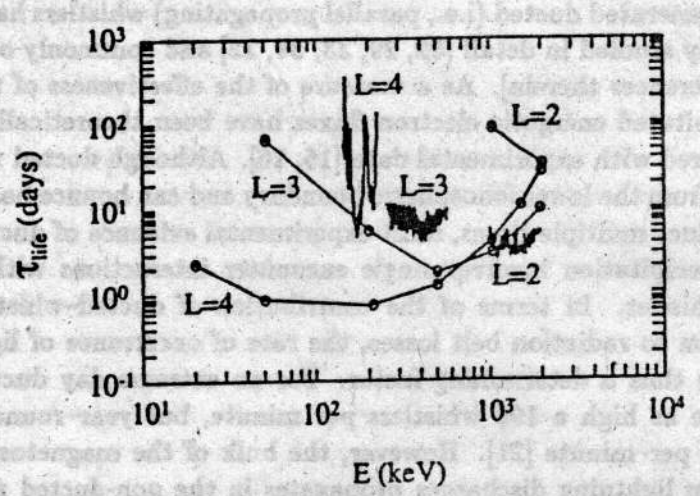

Fig.9. Electron lifetimes compared with previous work. We compare our lifetime estimates (—) with those due to cyclotron scattering by whistler mode hiss following large magnetic storms [1] (-o-).

CONCLUSIONS

We have carried out test particle simulations of the cyclotron resonant scattering of radiation belt electrons in a single resonant encounter (one pass) with obliquely propagating monochromatic whistler-mode waves in the magnetosphere. Our results indicate that, for typical parameters as used in this paper, these interactions result in significant perturbations of the trapped particle distributions and lead to precipitation of particle fluxes into the ionosphere. Although our individual simulations were limited to one-pass interactions with monochromatic oblique waves, when viewed as a whole, they imply that wave energy injected into the magnetosphere by lightning and propagating obliquely in the non-ducted mode may substantially contribute to the establishment of radiation belt equilibrium.

In this context, we have shown that oblique MR waves which settle down on given L-shells and exist for up to 100 s can significantly affect the lifetimes of the energetic electrons. In the case of the latter, in should be noted that non-ducted whistlers injected into the magnetosphere typically have components over a wide range of frequencies, so that each frequency component would

'settle' on a different L-shell and the scattering (as computed) can be expected to occur simultaneously over a broad range of L-shells during the 10–100 s following each lightning discharge.

The implications of our results should be evaluated in the context of recent theoretical and experimental findings which clearly indicate that ducted whistler waves originating in lightning regularly precipitate energetic radiation belt electrons. The ionospheric signatures of the scattering of energetic electrons out of the radiation belts in cyclotron resonant interactions with lightning-generated ducted (i.e., parallel propagating) whistlers has been both theoretically studied in detail [32, 29, 33, 34, 12] and commonly observed [13, 14, and references therein]. As a measure of the effectiveness of this interaction, precipitated energetic electron fluxes have been theoretically estimated and compared with experimental data [15, 16]. Although ducted whistlers often reflect from the lower ionospheric boundary and can bounce back and forth along the duct multiple times, most experimental evidence of ducted whistler induced precipitation involves single encounter interactions with a discrete one-hop whistler. In terms of the contribution of ducted-whistler-induced precipitation to radiation belt losses, the rate of occurrence of lightning and whistlers is thus a determining factor. For an extreme day ducted whistler rate can be as high a 195 whistlers per minute, but year-round average is 6 whistlers per minute [21]. However, the bulk of the magnetospheric wave energy from lightning discharges propagates in the non-ducted mode. Non-ducted whistlers do not require the presence of any specific density structures (e.g., ducts) for their propagation and they generally occupy larger regions of the magnetosphere [20]. On this basis, although the statistics of the occurrence rates of non-ducted whistlers are not well documented, it may safely be assumed that they occur at least as often as ducted whistlers.

Interaction of radiation belt electrons with MR whistlers at a later stage of their propagation (after the settlement of ray paths on a certain L-shell, when the wave normal angle is high, close to 90°) endures for as long as the waves exist ($\sim$ 100 s) so that it is appropriate to discuss the consequences of the losses in terms of radiation belt electron lifetimes. Interactions with MR whistlers causes precipitation of higher energy electrons from lower L-shells. Electrons in the energy range of 1–2.6 MeV are precipitated from $L = 2$, whereas from $L = 4$ precipitated electron energy range is 150–220 keV. The precipitated differential electron flux, due to this interaction, is higher for higher L-shells, and the maximum value is ranging from $\Phi_{E_{\text{prec}}}(1.11\,\text{MeV}) = 5.2 \times 10^{-4}$ el/cm^2·s·keV at $L = 2$ to $\Phi_{E_{\text{prec}}}(173\,\text{keV}) = 4.6 \times 10^{-1}$ el/cm^2·s·keV at $L = 4$. The lifetimes of the radiation belt electrons in a tube around the L-shell on which the interaction takes place range depending on electron energy from several days to $\sim$ 100 days and are comparable with lifetimes corresponding to electron loss induced by hiss [1]. The minimum electron lifetimes vary from 2.47 days for $E = 1.11$ MeV electrons at $L = 2$ to 4.64 days for $E = 173$ keV electrons at

$L = 4$.

REFERENCES

1. Lyons L.R., Thorne R.M. and Kennel C.F. //J. Geophys. Res. 1972. V.77. P.3455.
2. Dungey J.W. //Planet. Space Sci. 1963. V.11. P.591.
3. Rosenberg T.J., Helliwell R.A. and Katsufrakis J.P. //J. Geophys. Res. 1971. V.76. P.8445.
4. Helliwell R.A., Katsufrakis J.P. and Trimpi M.L. //J. Geophys. Res. 1973. V.78. P.4679.
5. Foster J.C. and Rosenberg T.J. //J. Geophys. Res. 1976. V.81. P.2183.
6. Lohrey B. and Kaiser A.B. //J. Geophys. Res. 1979. V.78. P.2142.
7. Helliwell R.A., Mende S.B., Doolittle J.H., Armstrong W.C. and Carpenter D.L. //J. Geophys. Res. 1980. V.85. P.3376.
8. Mende S.B., Arnoldy R.M., Cahill L.J. Jr, Doolittle J.H., Armstrong W.C. and Fraser-Smith A.C. //J. Geophys. Res. 1980. V.85. P.1194.
9. Rosenberg T.J., Siren J.C., Mathews D.L., Marthinsen K., Holtet J.A., Egeland A., Carpenter D.L. and Helliwell R.A. //J. Geophys. Res. 1981. V.86. P.5819.
10. Dingle B. and Carpenter D.L. //J. Geophys. Res. 1981. V.86. P.4597.
11. Carpenter D.L. and LaBelle J.W. //J. Geophys. Res. 1982. V.87. P.4427.
12. Chang H.C. and Inan U.S. //J.Geophys. Res. 1985. V.90. P.1531.
13. Inan U.S., Knifsend F.A. and Oh J. //J. Geophys. Res. 1990. V.95. P.17217.
14. Burgess W.C. and Inan U.S. //Geophys. Res. Lett. 1990. V.17. P.259.
15. Inan U.S., Chang H.C., Helliwell R.A., Imhof W.L., Reagan J.B. and Walt M. //J. Geophys. Res. 1985. V.90. P.359.
16. Inan U.S. and Carpenter D.L. //J. Geophys. Res. 1987. V.92. P.3293.
17. Inan U.S., Walt M., Voss H.D. and Imhof W.L. //J. Geophys. Res. 1989. V.94. P.1379.
18. Edgar B.C. //J. Geophys. Res. 1976. V.81. P.205.
19. Draganov A.B., Inan U.S., Sonwalkar V.S. and Bell T.F. //Geophys. Res. Lett. 1992. V.19. P.233.
20. Sonwalkar V.S. and Inan U.S., to be submitted to //J. Geophys. Res. 1993.
21. Burgess W.C. and Inan U.S. //J. Geophys. Res. 1992, in press.
22. Inan U.S. and Bell T.F. //J. Geophys. Res. 1977. V.82. P.2819.
23. Inan U.S. //J. Geophys. Res. 1987. V.92. P.127.
24. Jasna D., Inan U.S. and Bell T.F. //Geophys. Res. Lett. 1992. V.19. P.1639.
25. Angerami J.J. and Thomas J.O. /J. Geophys. Res. 1964. V.69. P.4537.

26. Park C.G. Methods of Determining Electron Concentrations in the Magnetosphere from Nose Whistlers. — Stanford: Radioscience Laboratory, Stanford Electron.Labs., Stanford Univ., 1972.
27. Inan U.S., Bell T.F. and Helliwell R.A. //J. Geophys. Res. 1978. V.83. P.3235.
28. Schield M.A. and Frank L.A. //J. Geophys. Res. 1970. V.75. P.5401.
29. Inan U.S., Bell T.F. and Chang H.C. //J. Geophys. Res. 1982. V.87. P.6243.
30. Bell T.F., Inan U.S. and Helliwell R.A. //J. Geophys. Res. 1981. V.86. P.4649.
31. Stix T.H. the Theory of Plasma Waves. — New York: McGraw–Hill, 1962.
32. Inan U.S. Non-Linear Gyroresonant Interactions of Energetic Particles and Coherent VLF Waves in the Magnetosphere. — Stanford: Radiosci. Lab., Stanford Electron. Labs., Stanford Univ., 1977.
33. Chang C.H. Cyclotron Resonant Scattering of Energetic Electrons by Electromagnetic Waves in the Magnetosphere. — Stanford: STARLAB, Stanford Electron. Labs., Stanford Univ., 1983.
34. Chang H.C. and Inan U.S. //J. Geophys. Res. 1983. V.88. P.10053.

LOLA Research Center, Belgrade,
Yugoslavia;
STAR Lab, Stanford University,
USA

Поступила в редакцию
22 ноября 1993 г.